Design and experiments on a continuous deformation soft manipulator module

João Maria Salgueiro
joao.maria.salgueiro@tecnico.ulisboa.pt
Instituto Superior Técnico
Universidade de Lisboa
Lisboa, Portugal
Janeiro 2021

***Abstract*—This article describes the work undertaken in the development and testing of a soft robot with an improved torsional stiffness capable to withstand torsional loads. The design of the manipulator was based on a wave spring that allows an increment of its torsional stiffness while maintaining its capacity to extend and compress. The number of waves per level was obtained from a static and dynamic finite element analysis. With all the parameters defined the elements were modelled and 3D printed with rigid and flexible filaments. Several experimental tests were performed. The first test obtained the work volume, the second test evaluated the repeatability of the manipulator, and lastly, a static and dynamic loading test was performed. In the end three trajectories were applied to the inverse kinematics models obtained from the training of neural networks. These models can be divided into: models trained with a varied number of data points from the theoretical model; models trained also with a varied number of data but from the manipulator; and models trained with all the manipulator data but with a variable number of neurons. From this study it was possible to design a structure for a continuum soft robot able to maximize its torsional stiffness without a significant loss of degrees of freedom. It was also demonstrated that a soft robot is capable to have an off-axis loaded motion with a considerable weight.**

***Index Terms*—Soft Robots, Continuum robots, Wave spring, Additive manufacturing, Neural Networks**

I. Introduction

Nowadays, robots play a significant role in the world around us, they are present in the most diverse areas of work not only from medicine, [1] - [6], to the manufacturing industry, [7], but also in our day-to-day life.

The majority of robotic manipulators is made of rigid structures, this feature is of paramount importance in order to obtain precise, strong, reliable and durable robots. In the manufacturing industry the use of robots have gained an increased importance in the most diverse assembly lines. These industrial robots are characterized by their precision and accuracy, their discrete rigid links, their considerable weight and required clearance volume to operate. Nonetheless, if they happen to operate alongside humans or any other living form some of these characteristics may raise security concerns. These discrete and rigid robots tend also to have some limitations when interacting with its surrounding environment, when in constrained, unstructured or delicate scenarios, [8].

The constraints previously mentioned can be overcome with a different approach based on continuum robots. This type of robots can be defined as a continuously bending robot without any rigid links and identifiable rotational joints, [9] - [11]. Continuum robots, due to its architecture, are able to exploit situations where neither the robots with rigid structure nor the humans are capable to operate, these include scenarios in unstructured and constrained environments. One of the reasons is that these robots are considered to have an infinite number of degrees of freedom (DOF) and since not all DOF are actuated, the robot will exhibit some form of passive compliance. Despite this passive compliance displayed appearing to be a disadvantage when tasks with precision and accuracy are required, it becomes a valuable asset for safer interactions and in fragile environments, [10].

Like everything that humans build, biology has always been a source of inspiration and the field of continuum robots follows suit. The inspiration to this field can be drawn from animals and plants as they result from an evolution with millions of years. Biology may then be considered an important source of intellectual material to be used in engineering, from the design of a bullet train mimicking a kingfisher's peak to a tentacle inspired soft robot, [12], [13].

An alternative to the usual rigid structures for the continuum robots, with inspiration drawn from biology, can be accomplished with soft materials. Soft robots, as they are called, use soft materials as its structure and main body instead of the usual discrete rigid links. With these softer materials the robot inherits several of its characteristics, namely its softness and flexibility. These inherited properties allow the soft robot to have a safe interaction when handling fragile and soft elements, and when operating in a delicate environment without the need to have a range of sensors and a complex controller, [14]. These materials are able to absorb external forces and deform accordingly with the contact surface, [13].

Soft continuum robots have been studied in the last years, [15] - [17], and one of the main posed challenge is the off-axis manipulation. Since the material of a soft manipulator is malleable it does not have a significant torsional stiffness and so may result in undesirably large deformations when in off-axis scenarios. In [17] it is proposed a pneumatic structure reinforced with an elastomer structured inspired by a wave spring geometry.

In this paper it is presented a similar 3D printer soft

continuum manipulator design and inspired by a wave spring structure capable to sustain torsional and off-axis loads. Contrary to [17] the present manipulator does not have a pneumatic actuator to extend and compress, instead it is actuated by semi-rigid cables.

The main contributions from this work are as follows: the design and construction, using almost fully automated procedures, of a soft continuum manipulator module capable to sustain torsional loads; a lightweight and fully working prototype actuated by semi-rigid elements (cables); an optimization of the number of waves per level of the wave spring based on simulation results; an off-axis manipulation capable to sustain loads with more than 4 times the module weight; the use of an additive manufacturing process, 3D printing, to produce a soft continuous module; a characterization of the model repeatability, with a mean radius of 2.98 mm, and of motions in off-axis scenarios with several loads without any fatal deformation; and finally, a first approach to the modelling of inverse kinematics using neural networks with a variable number of training points and neural networks with a variable number of neurons in order to obtain the minimum number of training points and the evolution of the modulation of nonlinearities according to the neurons used. Both resultant mean errors are in the same order of magnitude as the repeatability radius.

Part of the work developed here resulted in a paper accepted for publication in an international conference, [18].

II. DESIGN AND ANALYSIS

The design of the manipulator is a product of several requirements and practical constraints. The most important requirement to be fulfilled is the necessity to have an increased torsional stiffness able to resist torsional and off-axis loads. The geometry chosen due to its torsional stiffness was the wave spring. To take fully advantage of this design all the elements that compose the prototype should be delimited by the volume of the spring and cable driven. This manipulator is also required to bend at least 90º. On the other hand, the 3D printing of the flexible module may constrain some parameters of the wave spring. The analysis and fabrication of the module were developed simultaneously with several iterations. As a result of being cable driven with 3 actuators, the number of waves per level should be a multiple of it to maintain the symmetry.

A. Static and Dynamic Analysis

Almost all the parameters were defined according to the functional constraints of both the fabrication method and the requirements for a functional manipulator. The number of waves per level is the only parameter still undefined. For that it was realized a finite element analysis to obtain the model with the greatest torsional stiffness in relation to the extensional and bending stiffness. The models used in the simulations can be seen in the figure 1 with 3, 6 and 9 waves. The material used was *FilaFlex*™ from Recreus Industries S.L.™ (tensile storage modulus: 48 MPa, density: 1200 kg/m^3, Poisson's ratio: 0.49).

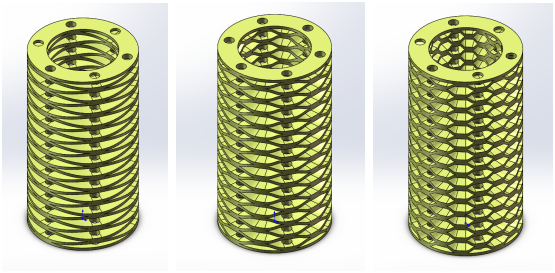

Fig. 1. Wave spring structure with 3, 6 and 9 waves per level respectively

For the static simulation the three models had a constrained displacement at the base, and were subjected to four types of loads: extension and compression forces, axial torque, and a transverse force, all applied at the top section. The results of stiffness for each model and load case can be analysed in table I. The extension and compression forces are a direct result of the maximum applied torque by the actuators.

TABLE I
SPRING STIFFNESS FOR SEVERAL LOAD CASES

	Test A (Extension)	Test B (Torsion)	Test C (Transverse)
3 Waves	29.482 N/m	1.345 Nm/rad	No reliable data
6 Waves	747.496 N/m	6.158 Nm/rad	59.242 N/m
9 Waves	5051.015 N/m	9.155 Nm/rad	403.226 N/m

	Test D (Compression)
3 Waves	29.542 N/m
6 Waves	748.951 N/m
9 Waves	5056.6345 N/m

The results in figure 2 show a better torsional stiffness to extension and bending stiffness for the module with 6 waves. Such result can be a result of two factors, the resulting material density and the maximum angle of the wave relative to the base plane. The first is a resultant of the increase number of waves while maintaining all the remaining parameters. The second is a consequence of decreasing the period wave, as the number of waves increases so does the maximum angle made by the wave. These factors can be observed in figure 1 where the angle evolution and the increased density is seen. With a lower angle the model will have a lower compression and extension stiffness and a more vertical wave will have a higher compression and extension stiffness. The increasing angle will result in a minor increment of torsional stiffness when compared to the extending and bending stiffness. The model with 6 waves presents a longitudinal stiffness 6.8 times inferior to the model with 9 waves but a torsional stiffness only 1.5 times inferior. In comparison to the model with 3 waves the manipulator increases 25,4 times the extension and compression stiffness and has an increment of 4.6 times for the torsional stiffness. The manipulator with 3 waves showed to have a weak compression stiffness to support its own weight. Therefore the model chosen was with 6 waves per level.

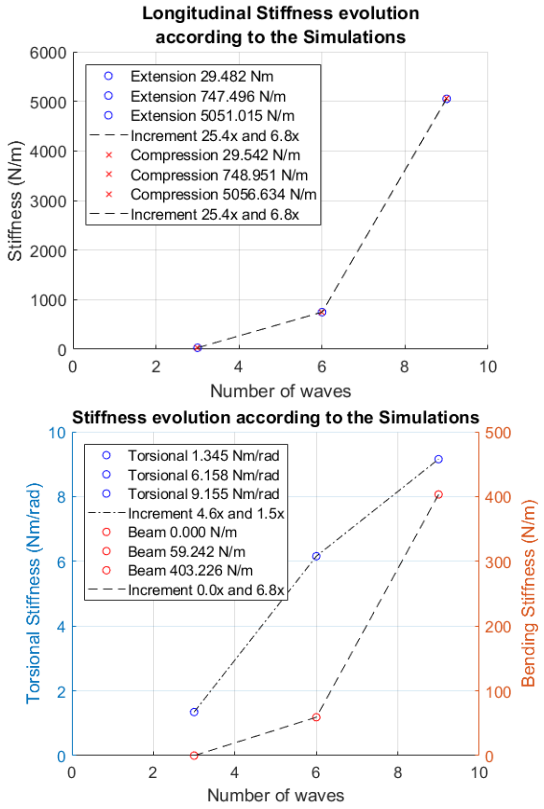

Fig. 2. Evolution of the stiffness with respect to the number of waves per level

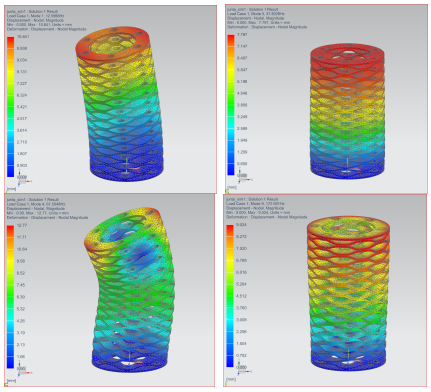

Fig. 3. Mode shapes from modal analysis. From the top left in clockwise direction: 1st mode (1st bending), 3rd mode (extension), 9th mode (torsion) and 4th mode (2nd bending).

TABLE III
FINAL MEASURES OF THE MODULE

Length	84.5 mm
Inner Diameter	29.5 mm
Outer Diameter	45.5 mm
Number of wave levels	26
Wave thickness	1.25 mm
Wave amplitude	1.90 mm
Contact area between waves	4 mm
Number of waves per level	6
Number of guiding holes	6
Diameter of the guiding holes	4.25 mm

A modal analysis was performed for the model with 6 waves, and the most important natural frequencies are shown in table II, the corresponding mode shapes are displayed in figure 3. Under dynamic loads the torsional stiffness has a natural frequency considerably higher than the bending and extension modes, a result in accordance with the aim of the work and with the previous results.

TABLE II
MODAL MODES AND FREQUENCIES

Mode	Type	Frequency
Modes 1,2	1st Bending mode	12 Hz
Mode 3	Extension	37 Hz
Modes 4,5	2nd Bending mode	61 Hz
...	...	...
Mode 9	Torsion	172 Hz

III. PROTOTYPE DESCRIPTION

The final dimensions that were used to 3D print the wave spring and produced the best results after 3D printed are shown in table III

The final prototype and remaining elements elements can be seen in figure 4 alongside the experimental setup. In the figure on the right it is also seen several parts printed in a rigid filament, PLA. These include: a tip element that clamps the cables; several clamps to attach this top element to the flexible module; clamps to attach the flexible module to the base plate; and the servo mounts with the pulley to drive the cables. Nylon tubes with a inner diameter of 2 mm were added to the pass-through holes in the wave spring to reduce the friction.

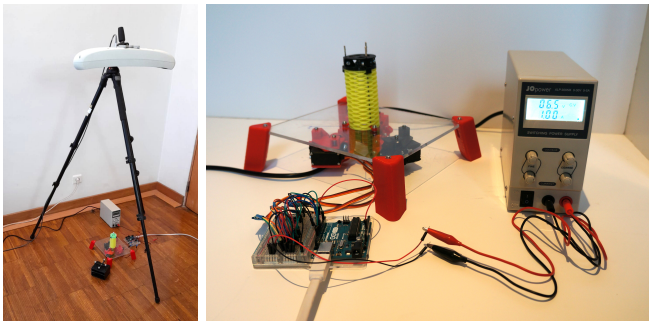

Fig. 4. Experimental set-up and components.

The actuators, in 5, convert the rotational motion to a linear actuation using an enclosed pulley where the cable is pulled and pushed. The lid, top element in red, locks the cables to transfer the motion from the cables to the manipulator. Although this design can be improved for both friction and durability, no significant friction forces or wear were found during these experiments, and no lubricant was used.

Due to the design and work that the top clamps will be subjected, a finite element analysis was also made to these.

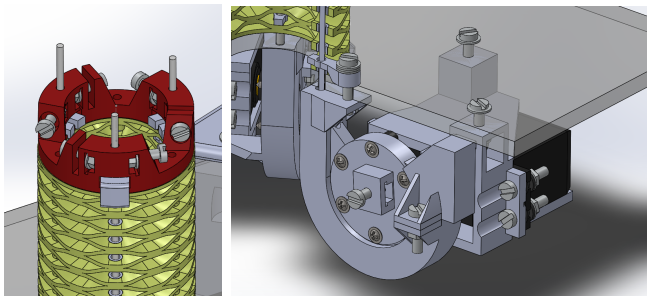

Fig. 5. Motor and cable assembly details.

Figure 6 show the expected concentration of stress on its inner face with a 34,88 MPa. This value is very similar to the tensile strength at break when the force is perpendicular to the printing layers with 39 MPa. However, if the force is applied in the same direction of the layers this value increases to 50 MPa. For such reason this element should be 3D printed sideways.

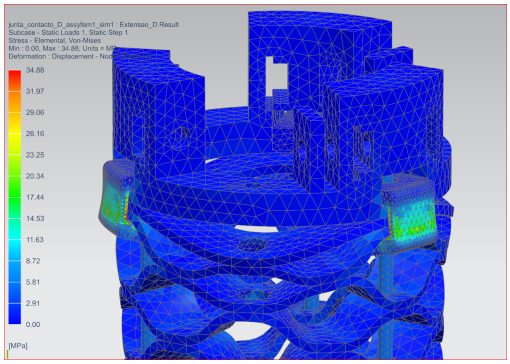

Fig. 6. Motor and cable assembly details.

In the process of 3D printing the rigid parts of the module there weren't experienced any major difficulties since PLA is one of the most easiest material to print with. However, when it comes to the soft spring a more cautious approach was needed. Several prototypes were produced in order to allow and refine the 3D printer parameters for the *FilaFlex*™ filament.

The hardware required to perform the experiments can also be seen in figure 4 and consists of:

- Embedded controller - Arduino ™ UNO Rev3
- Power Supply - Jopower™ ALP-3005M 0-30V 0-5A
- Servo Motors - Tower Pro™ MG996R
- 3D Tracking System - Polaris Spectra™

Two sets of markers are used with the 3D Tracking System: one attached to the base plate to provide the global reference frame ($O_P - X_P Y_P Z_P$), and a single marker at the tip of the robot module to track its position ($O_2 - X_2 Y_2 Z_2$). Data acquisition from the Polaris Spectra™ system was accomplished by using the manufacturer's own software.

IV. Kinematics

To control a robotic manipulator it is necessary to obtain a forward and an inverse kinematic model that approximates the manipulator behaviour. The first gives the end-effector position when the inputs of the actuators are defined. While the second gives the inputs required for the end-effector to reach a desired position.

For the computation of the forward kinematics it was used the constant curvature theory that assumes that the module has a perfect curvature when bent. Some model formulations can be found in, for instance, [10], [11], [13], [19]. Later it was added an offset to this theory to better approximate it to the assembled prototype.

The inverse kinematics for the constant curvature theory with an added offset, relative to the rigid part at the top of the model, is more complex so a different approach to the mathematical one is required. For that, it was used neural networks. This first approach to the neural networks allows to, besides obtaining the inverse kinematics for the theoretical model, prepare for the training of the neural networks using the data collected from the prototype. The neural networks architectures used for the inverse kinematics of the constant curvature model and the prototype followed the architectures from [20]. With 3 inputs, Cartesian position, 3 outputs, actuators position, 1 hidden layer with 100 neurons and sigmoid activation function, and an output layer with a linear activation function. The neural network was created using a toolbox from *Matlab*, trained with the Levenberg-Marquardt backpropagation algorithm and evaluated with the mean-squared error. The samples were divided in 70% for training, 15% for validation and the last 15% for testing.

The first networks were created for the constant curvature model and for training them it was necessary to generate training data. For this, 1000 input data was randomly generated and the respective output was obtained using the forward kinematic model. Next, the models were trained with a variable number of training points, 100 from 100 to 1000. The resultant R evolution, value that measures the relation between the inputs and outputs, is demonstrated in figure 7, as well as the R evolution for other models that will be explained later. A value of R closer to 1 means a closer relationship and less randomness.

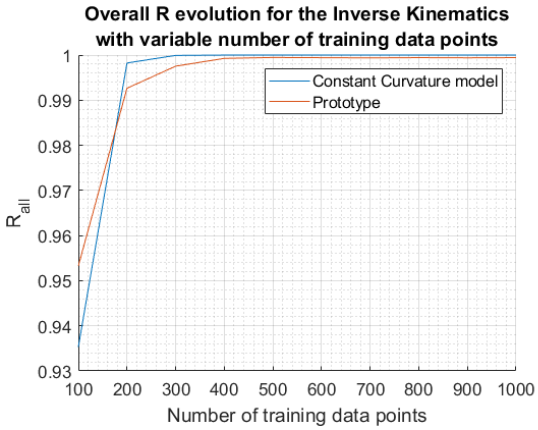

Fig. 7. Overall R evolution for neural networks trained with theoretical and experimental data

With the inverse kinematic models it was calculated the inputs from three different trajectories, and then applied to the simulated manipulator using its forward kinematics. From the several trajectories obtained it was possible to calculate the mean and maximum error evolution according to the number of training points. The first is seen in figure 8 while the second shows a similar evolution to the first.

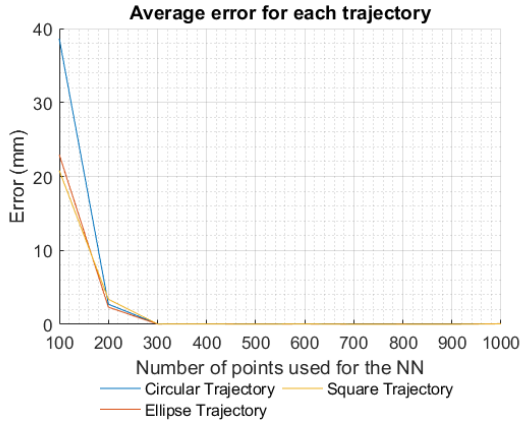

Fig. 8. Average error evolution for the models trained with theoretical data

From the two graphics referenced earlier, figures 7 and 8, it is possible to relate the R evolution with the mean error evolution. It is possible to state that as soon as R stabilizes at its maximum, the mean error ceases to decrease significantly. From the model with 300 training points onwards the mean error of all trajectories varied between 0.015 and 0.085 millimeters. From this it is possible to validate the neural network architecture and so train it with the data acquired from the prototype. The respective R evolution can be also visualized in figure 7. With these values and the previous conclusion it is possible to assume that the minimum number of points to train correctly the model will be greater than 400. The error evolution can be seen in the next section.

After the examination of the mean error and the paths from the previous neural networks, in the experimental part, it was made an attempt to improve the performance of the manipulator. For that, the number of neurons was varied in the hidden layer, to 25, 50, 75, 150 and 200 neurons, while using all the training data collected for the previous models. From the R evolution it is not possible to reach a clear conclusion for the expected error evolution as it only shows a slightly decreasing trend in a small range (approximately between 0.9993 and 0.9995).

V. RESULTS AND DISCUSSION

In the present section it will be shown and discussed the most important results obtained. These include: the experimental work volume; repeatability results from the prototype; static and dynamic loading tests; and the trajectories obtained from the inverse kinematic models trained with neural networks.

A. Passive Compliance

Figure 9 shows the resultant displacement, in an s-shape, of the manipulator after a lateral force is applied to the manipulator on a vertical position. It is noticed that even though the force is applied to the top face, this will not bend but rather maintain approximately the same direction and move almost parallel to it.

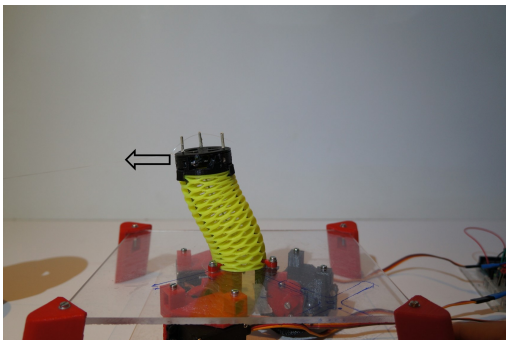

Fig. 9. Passive compliance after a lateral force is applied

B. Experimental Work Volume

In the graphs presented here, figure 10, it is possible to analyse several lines. Two of them represent the perfect constant curvature model and result from its forward kinematics. One of them represents the origin of the extremity of the flexible module while the other represents the offset added. This added offset accounts to, besides the pieces needed to assemble the prototype, an offset added to prevent the marker from being hidden by the manipulator own body.

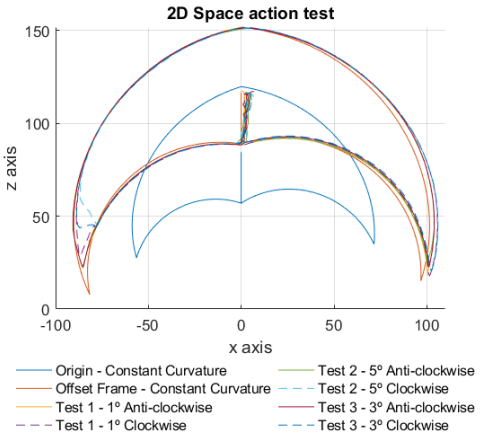

Fig. 10. Obtained 2D action space with constant curvature model

The greatest errors in the trajectories occurs in the two lowest points of both sides where the curvature is greater. This difference can be a result of a non perfect curvature area in both the top and base of the module due to the added elements.

C. Repeatability

Repeatability is an important property for a manipulator, the definition of repeatability used was based on [21], where it was applied to an industrial manipulator.

Three different tests were developed to analyse different aspects of the manipulator behaviour. The experiments were conducted with 5 randomly generated inputs, maintained throughout the tests, with each cycle repeated 10 times. The first test studies the repeatability of every point when originated from the rest position and the impact that the reached position has on the neutral point, (N $\rightarrow$ P_i $\rightarrow$ N). In the second test the manipulator follows the numerical order of the generated positions, (N $\rightarrow$ P_1 $\rightarrow$ P_2 $\rightarrow$ P_3 $\rightarrow$ P_4 $\rightarrow$ P_5 $\rightarrow$ N). In this test it is maintained the initial position for each point, however the initial position will not be the same for every point as it is dependent of the numerical order. Finally, the last test is very similar to the second one, however it follows a random order for each of the 10 cycles. For each of the cycles the first and last positions were also the neutral pose.

The average error evolution for the three tests and the different positions can be examined in figure 13.

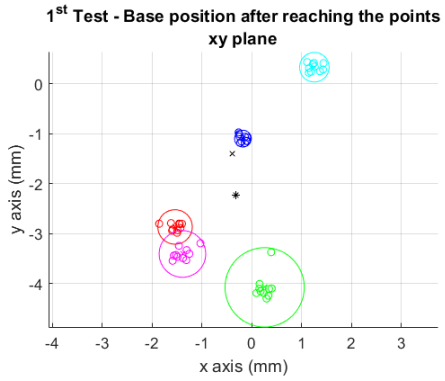

Fig. 11. Position of the origin from the first test

The results of the first test show a good repeatability with an average radius of 0.35 millimeters for the end positions and 0.41 mm for the origin. Besides this good repeatability, it is possible to observe a clustering of points sorted by the reached position. Figure 11 shows the clustering of the neutral position where each cluster is slightly pulled to the direction of the destination point, each color matches to the destination points in 12. This scattered clusters can be a result from the manipulator hysteresis. The second test shows similar results, with an average repeatability radius of 0.53 mm and an increment of 40.5%. This result reinforces the theory that if the path is maintained constant the repeatability will be good as the impact from the hysteresis is constant.

In the third and final test, figure 12, the radius for each point increases significantly, about 456.5% with an average of 2.98 mm and a median of 2.69mm. Such increase can be linked to the random order that the manipulator follows and to the varied displacement resultant from the manipulator hysteresis when the motion is originated from different locations.

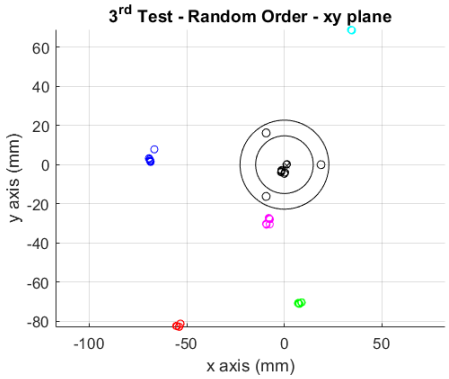

Fig. 12. Position of the points following a random order

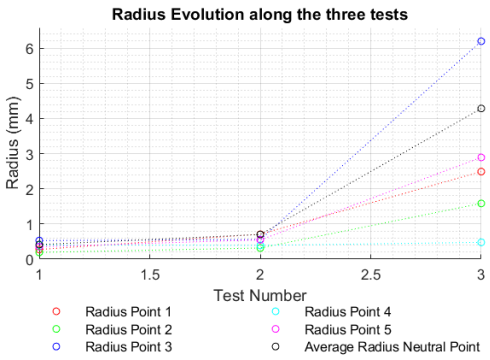

Fig. 13. Repeatability evolution according to the tests realized

D. Loading Experiments

To verify the improvements of this geometry, regarding the torsional stiffness and off-axis manipulation, it was realized two loading experiments with several weights. A static and a dynamic experiment were conducted with the setup seen in the next figure. The weights used in the next tests were: 0g, 50g, 100g and 150g.

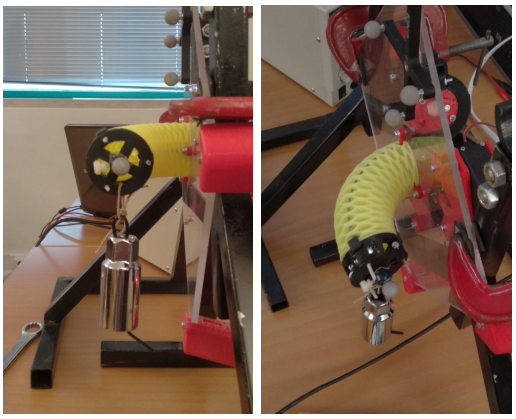

Fig. 14. Vertical base mount for the static loading set-up

1) Static Loading: In this first experiment the manipulator is submitted to weights in four different poses. The poses considered are: 1) the original undeformed shape, neutral; 2)

a fully extended (with a tip displacement of 35.4mm from the neutral pose); 3) a fully compressed (with a tip displacement of 28.4 mm from the neutral pose); 4) and a bent pose with a rotation of the top face of 99.5º and an increment of the neutral line length from the neutral position of 8.1 mm, seen in figure 14. The tip displacement was measured along the vertical axis (y) after the different weights were added to the tip of the manipulator, this displacement can be seen in the figure 15. From these values and from the weight added it was possible to calculate the resultant stiffness of the different poses in figure 16.

Fig. 15. Displacements from the static loading test for several tip loading conditions: 0 (baseline), 50, 100 and 150 grams.

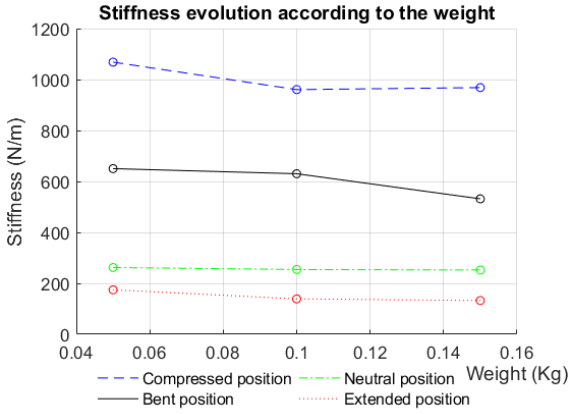

Fig. 16. Stiffness estimated from the static loading test for several tip loading conditions: 50, 100 and 150 grams.

From the experiment results it is noticed that even though the neutral line length is larger in the bent pose than on the neutral position, the displacement on the first is smaller and its stiffness is more than two times greater. Another important aspect is that the module has a weight of 36g and is able to support loads 4 times larger. This result demonstrates the capacity to sustain torsional and off-axis loads.

2) Loaded Trajectory Tracking: This second loading experiment aims to verify the results so far obtained and guarantee that the previous conclusion also applies to dynamic motions. Two trajectories were applied, a circular in figure 17 and an elliptical. The inverse kinematics to compute the inputs of the trajectory were obtained from the constant curvature without offset. The results in figure 17 display in light blue the desired trajectory. It is noted that it does not only show a vertical displacement, as expected, but also a displacement along the z axis. In the second image of the referenced figure it is possible to deduct that as the weight added increases so does the diagonal observed in the figure. Such behaviour might be a consequence of the passive compliance as explained before resulting in a sideways movement. When the manipulator has a slightly upwards orientation the tip, due to the applied weight, will move downward (according to the vertical direction) and, to follow the face orientation will move forwards (according to the z axis). If the manipulator has a slightly downwards orientation it will also move downward but backwards. The base of the manipulator is at the plane xy. Nonetheless, the results obtained show a good and consistence performance with off-axis manipulation.

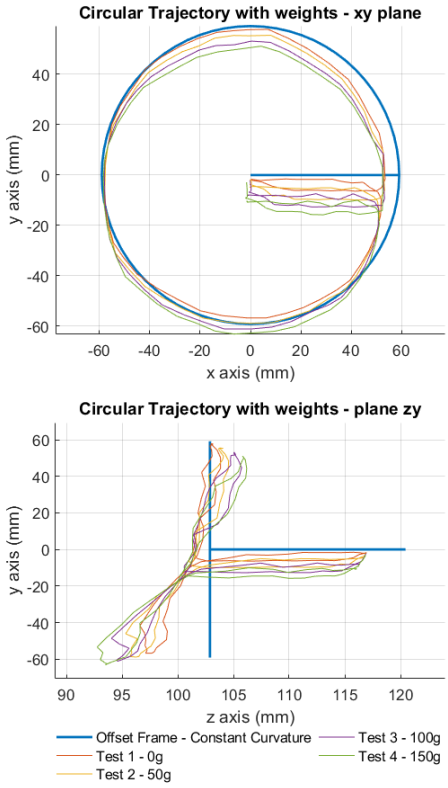

Fig. 17. Circular trajectory experimental results. The z axis is coincident with the axis of the robot module in its unbent configuration, the y axis corresponds to the direction of gravity.

E. Trajectories

With the obtained models from the inverse kinematics it was possible to calculate the inputs for three different trajectories for each model. It was then calculated the mean and maximum error from the obtained trajectories according to the number of

training points. Figure 18 illustrates the average error evolution for the models created with the constant curvature model and for the models created with the collected data from the manipulator.

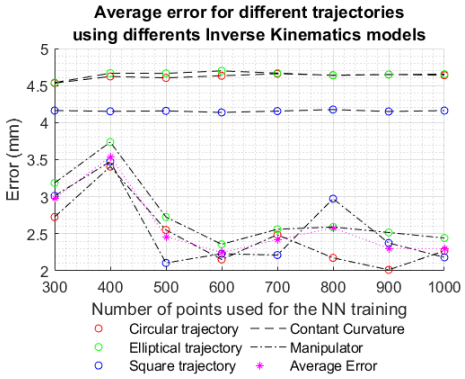

Fig. 18. Mean error for 3 trajectories for models with different numbers of training data points

The error for the theoretical model is constant since, as seen in kinematics, the required number of points to train correctly the manipulator is 300, and from this model on, the models will be very similar and produce similar results. From the models trained with the collected data from the prototype the error is inferior and seems to stabilize after the model with 500 training points, with the exception of the square trajectory for the model with 800 points. Considering this evolution and the R evolution from figure 7 it is possible to state that the minimum number of training data points, for this neural network architecture, is from 500/600 as no significant improvement is made after these. According to the R evolution the error should stabilize after the model with 400 points, however it is not the case as this model shows a bigger error than the previous model and might be a result from an unfit training.

From the error evolution and the path described by the manipulator it is perceived that the model that better suits all trajectories is the model trained with 600 points. This model has an average error, from the three trajectories, of 2.24 mm. The remaining models, with the exception of the the model trained with 300 and 400 points, have a mean error that is in the range of 2.29 to 2.57 mm. This range is on the same order of magnitude as the random repeatability radius test, which leads to conclude that the neural networks were trained correctly for the current setup.

Nonetheless, it was still attempted to improve the results so far obtained with a different neural network architecture. From these new models, with the error evolution in the next figure, it is possible to see a small increase on the mean error evolution. Such result can be linked to the rate of compensation of the models nonlinearities.

Figure 20 shows the most clearer evolution among the models with variable number of neurons, on the left and right sides of the square trajectory. From left to right: it shows a trajectory obtained with the theoretical model, a trajectory

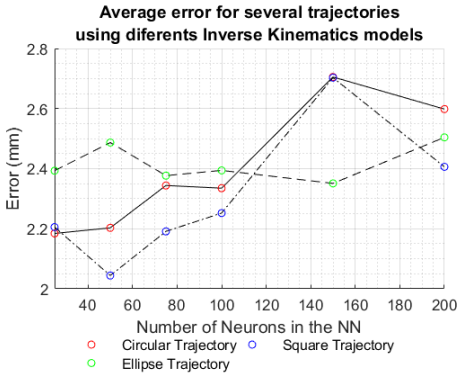

Fig. 19. Mean error for 3 trajectories for models with different numbers of neurons

obtained with a model with a low number of neurons (50), and a trajectory obtained from a network with the highest number of neurons (200). The model that apparently compensates better all nonlinearities is the model with 50 neurons.

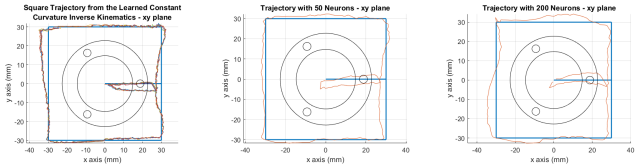

Fig. 20. Square trajectory. From left to right: theoretical model; model with 50 Neurons; And model with 200 Neurons.

VI. CONCLUSIONS

At the end of the work described in this paper it was successfully achieved the design, fabrication, modulation and experimental evaluation of a soft continuum manipulator capable to sustain torsional forces, improve the performance of this type of robots in off-axis scenarios and define improvement guidelines for further exploration in future works. Therefore the work is divided in two major parts: in design and in experimental sections.

On the first part it was optimized the design of the wave spring in terms of the number of waves per level in order to obtain the best torsional to extending and bending stiffness relation. The finite element analysis was performed on three different models with 3, 6 and 9 waves per level. The first model showed a small extending and compressing stiffness, crucial to support its own weight, as the wave angle with the base plane is small. In contrast, the third model has an extending and compressing stiffness too great as a result of a more vertical wave. It also has the largest torsional stiffness. The model with 6 waves showed a torsional stiffness only 1.5 times inferior to the larger torsional stiffness while having an extending and bending stiffness 6.8 times smaller regarding the same model. This model has also a torsional stiffness 4.6 times greater than for the model with 3 waves and an extension and bending stiffness 25.4 times larger, providing a good support for its own weight. A modal analysis was then performed on

the most suitable model with 6 waves. The resultant torsional stiffness has the largest natural frequency when compared with the remaining stiffness. The flexible module and the majority of the rigid elements were 3D printed with a flexible and a rigid filament respectively.

On the second part of this work, with the manipulator fully assembled, it was possible to evaluate its working volume, its behaviour with and without loads, its repeatability, and the trajectories resultant from several inverse kinematic models trained with neural networks. The working volume allowed to validate the theoretical model. The loading test provided an assurance that the module is capable to work with off-axis loaded motions. In the static loading test, 4 different weights were applied to the manipulator in 4 different poses, from these only one pose was off-axis. The obtained vertical stiffness of this pose was greater than two of the on-axis poses, only being smaller than the fully compressed pose. In the dynamic loading test the manipulator described a consistent and reliable motion with a load 4.16 times its own weight. The repeatability was obtained from two tests with a defined order and from a third test with a random order. For the first two the repeatability radius was very similar, 0.35mm and 0.53mm. While for the third test the radius increases significantly to 2.98 mm due to its random order. On the first test it is possible to visualize the effects of hysteresis by a clustering of points depending on the previously reached pose. This may be the reason why, with random order, the repeatability radius increases significantly. In the last experimental work it is possible to analyse the nonlinearities of the model present on the trajectories obtained from the models trained with the theoretical data. To analyse the evolution of the mean error according to the number of training points and obtain a minimum number of 500. And to evaluate the impact that the number of neurons have on the modulation of the manipulator. From the trajectories described, especially from the square trajectory, it was seen that as the number of neurons increase, the compensation rate of the nonlinearities also increase. The model that better followed the square trajectory was the model trained with 50 neurons.

VII. Achievements

The main accomplishment of this work was the design and construction, using almost fully automated procedures, of a soft continuum manipulator module capable to sustain torsional loads that allows to approximate this soft manipulator to a fully functional and useful robot.

Several other findings can be listed next:

1) Parameter optimization of a wave spring capable to sustain torsional forces and operate in off-axis scenarios;
2) The design of a lightweight with hollow center soft continuous manipulator;
3) A simple actuation method with few moving parts;
4) The combination of a 3D printing production method, using flexible filaments, with the necessity of quickly prototyping a soft continuous deformation robot;
5) A manipulator capable to sustain, without significant deformation, a weight of at least 4,16 times the module weight in static and dynamic scenarios;
6) The characterization of the manipulator work space and repeatability with a mean radius of 2.98 mm;
7) A first approach to modeling the kinematics of the prototype using neural networks, that includes a study of the number of training points required to effectively model it (500) and the impact of the number of neurons used (from 25 to 200, with the first ones obtaining the best results).

This geometry is a step further for the soft robots to be commonly used in more diverse areas. 3D printing can be extremely helpful in future developments of soft robots, however it may not be the answer if the manipulator will be subjected to extreme stress scenarios where the material can malfunction due to the method of printing by layers, or if the aim is to mass produce. Regarding neural networks and artificial intelligence, they are a valuable tool to model behaviours that may be too complex for detailed modelling by other means and were an important asset for the prototype here created.

VIII. Future Work

This work might be a starting point for future works that can follow multiple directions according to the selected project goals.

1) A first area that can be improved is the characterization of the materials used and a research into alternative materials to these. This study can also help choosing a material that minimizes the hysteresis of the flexible module. Next, it can be examined the resultant properties of the 3D printed elements;
2) Another possibility for improvement is the design of the actuation mechanism in order to reduce the overall volume of the robot module. For this, linear actuators, or miniature actuators embedded in the structure of the link itself can be investigated;
3) Another area to be studied is the addition of proprioceptive sensors to the module to have a better perception of the robot curvature. This inclusion will allow a better control, accuracy and also to reduce the dependency of external sensors like the Polaris system used in this work;
4) Following the development of the single module, a full robot structure comprised of several modules can be assembled and studied, in order to develop both low level, and also high level behavioural control algorithms.

Acknowledgment

The author would like to thank Prof. João Reis for all the help and guidance provided during this work, Prof. Jorge Martins and researchers João Oliveira and João Gouveia for the help given in collecting the data.

REFERENCES

[1] T. Ranzani, G. Gerboni, M. Cianchetti, and A. Menciassi. A bioinspired soft manipulator for mini-mally invasive surgery.Bioinspiration & Biomimetics, 10(3):035008, may 2015.

[2] M. Manti, A. Pratesi, E. Falocito, M. Cianchetti, and C. Laschi. Soft assistive robot for personalcare of eldery people.IEEE RAS/EMBS International Conference on Biomedical Robotics andBiomechatronics, pages 833–838, June 2016.

[3] T. Branch, S. Stinton, M. Sterberg, W. Hutton, F. Lavoie, C. Guier, and P. Neyret. Robotic axial lowerleg testing:repeatability and reproducibility.Knee Surg Sports Traumatol Arthrosc, 23:2892–2899,2015

[4] Y.-J. Kim, S. Cheng, S. Kim, and K. Iagnemma. A stiffness-adjustable hyperredundant manipula-tor using a variable neutral-line mechanism for minimally invasive surgery.IEEE Transactions onRobotics, 30:382–395, 2014.

[5] Ranzani, T., Cianchetti, M., Gerboni, G., De Falco, I., and Menciassi, A. (2016). A soft modular manipulator for minimally invasive surgery: design and characterization of a single module. IEEE Transactions on Robotics, 32(1), 187-200.

[6] Burgner-Kahrs, J., Rucker, D. C., and Choset, H. (2015). Continuum robots for medical applications: A survey. IEEE Transactions on Robotics, 31(6), 1261-1280.

[7] Kolachalama, S., and Lakshmanan, S. (2020). Continuum Robots for Manipulation Applications: A Survey. Journal of Robotics, 2020.

[8] D. Trivedi, C. D. Rahn, W. M. Kier, and I. D. Walker. Soft robotics: Biological inspiration, state of theart, and future research.Applied Bionics and Biomechanics, 5(3):99–117, Sept. 2008.

[9] Robinson, G., and Davies, J. B. C. (1999, May). Continuum robots-a state of the art. In Proceedings 1999 IEEE international conference on robotics and automation (Cat. No. 99CH36288C) (Vol. 4, pp. 2849-2854). IEEE.

[10] R. J. Webster and B. A. Jones. Design and kinematic modeling of constant curvature continuumrobots: A review.The International Journal of Robotics Research, 29(13):1661–1683, 2010.

[11] Walker, I. D. (2013). Continuous backbone "continuum" robot manipulators. International Scholarly Research Notices, 2013.

[12] A. k. Goel. Biologically inspired design: A new program for computational sustainability.IEEEIntelligent Systems, pages 80–84, 2013.

[13] Boccolato, G., Manta, F., Dumitru, D., and Cojocaru, D. (2010). 3D kinematics of a tentacle robot. International Journal of Systems Applications, Engineering and Development, 4(1), 1-8.

[14] J.-Y. Lee, E.-Y. Go, W.-Y. Choi, W.-B. Kim, and K.-J. Cho. Development of soft continuum manip-ulator with pneumatic and tendon driven actuations.13th International Conference on UbiquitousRobots and Ambient Intelligence (URAI), pages 377–379, Aug. 2016

[15] Manti, M., Pratesi, A., Falotico, E., Cianchetti, M., and Laschi, C. (2016, June). Soft assistive robot for personal care of elderly people. In 2016 6th IEEE International Conference on Biomedical Robotics and Biomechatronics (BioRob) (pp. 833-838). IEEE.

[16] Wang, Y., and Lee, K. (2017, July). 3D-printed semi-soft mechanisms inspired by origami twisted tower. In 2017 NASA/ESA Conference on Adaptive Hardware and Systems (AHS) (pp. 161-166). IEEE.

[17] Skorina, E. H., and Onal, C. D. (2020). Soft Hybrid Wave Spring Actuators. Advanced Intelligent Systems, 2(1), 1900097.

[18] J. M. Salgueiro and J. C. P. Reis. Towards a highly integrated 3d printed soft continuum manipulator. ICARA - International Conference on Automation, Robotics and Applications, Accepted forpublication

[19] Rolf, M., and Steil, J. J. (2012, October). Constant curvature continuum kinematics as fast approximate model for the Bionic Handling Assistant. In 2012 IEEE/RSJ International Conference on Intelligent Robots and Systems (pp. 3440-3446). IEEE.

[20] A.-V. Duka. Neural network based inverse kinematics solution for trajectory tracking of a roboticarm.The 7th International Conference Interdisciplinarity in Engineering, pages 20–27, 2013

[21] M. PŁaczek and Ł. Piszczek. Testing of an industrial robot's accuracy and repeatability inoff and online environment.Eksploatacja i Niezawodnosc - Maintenance and Reliability, 20(3):455–464, 2018. http://dx.doi.org/10.17531/ein.2018.3.15.

[22] Cooper, T. G., and Anderson, S. C. (2008). U.S. Patent No. 7,320,700. Washington, DC: U.S. Patent and Trademark Office.